2016

Experimental Evaluation of Compressive Elastocaloric Cooling System

Suxin Qian
University Of Maryland, United States of America / Xi'an Jiaotong University, sqian@umd.edu

Yi Wang
University Of Maryland, United States of America, bill_wang_0102@hotmail.com

Yunlong Geng
University Of Maryland, United States of America, ygeng1@umd.edu

Jiazhen Ling
University Of Maryland, United States of America, jiazhen@umd.edu

Jan Muehlbauer
University Of Maryland, United States of America, muehlie@umd.edu

See next page for additional authors

Experimental Evaluation of a Compressive Elastocaloric Cooling System

Suxin QIAN[1,2], Yi WANG[3], Yunlong GENG[3], Jiazhen LING[1], Jan MUEHLBAUER[1], Yunho HWANG[1]*, Reinhard RADERMACHER[1], Ichiro TAKEUCHI[3]

[1]Department of Mechanical Engineering, University of Maryland
College Park, MD, United States
[2]Department of Refrigeration and Cryogenic Engineering, Xi'an Jiaotong University
Xi'an, Shaanxi, China
[3]Deparment of Materials Science and Engineering, University of Maryland
College Park, MD, United States
* Corresponding Author: Tel: 301-405-5247, Email: yhhwang@umd.edu

ABSTRACT

Elastocaloric cooling has been recognized as the most potential technology to compete with the state-of-the-art vapor compression cooling systems. The elastocaloric effect refers to the latent heat associated with the stress-induced martensitic phase transformation process in shape memory alloys (SMA). In this paper, the latest test results of a previously developed elastocaloric cooling system are demonstrated. Since the first generation prototype resulted in the system temperature lift of 1.5 K and cooling capacity of 38 W, the following system design modifications were made to improve system performance. Better alignment of linear actuator to SMA tubes enabled more SMA tubes per bed. Plastic tubing in loading heads reduced the heat loss. In addition, inserting plastic blocks inside SMA tubes reduced heat transfer fluid residing inside each Ni-Ti tube and reduced the cyclic loss associated with periodic heating and cooling of the heat transfer fluid. After applying these modifications to the system, the system temperature lift was improved to 4.7 K. Furthermore, 6.1 K system temperature lift was predicted when assuming no pump's parasitic heat generation and no heat conduction loss to the supporting frame in each bed.

1. INTRODUCTION

Elastocaloric cooling utilizes the latent heat released/absorbed from shape memory alloys (SMA) during stress induced martensitic phase transformation processes. It has been regarded as the most potential not-in-kind cooling technology by the Department of Energy (Goetzler et al., 2014). A few elastocaloric cooling prototypes have been reported worldwide, including designs without heat transfer fluid (HTF) to simplify the design (Saylor, 2012, Ossmer et al., 2015, Schmidt et al., 2015). Designs following the conventional magnetocaloric cooling prototypes were also discussed (Tusek et al., 2015). We have demonstrated the world's first of-its-kind compressive elastocaloric cooling prototype based on the single-stage reverse Brayton cycle with HTF, as illustrated by Figure 1 (Qian et al., 2016). The cycle requires at least two identical beds of SMAs as two beds are operated in batch mode to achieve a continuous cooling. The cycle starts by applying stress to the first bed from state 1 to state 2 adiabatically while simultaneously releasing the stress in the second bed from state 4 to state 5. Followed by the heat transfer process, the first bed rejects heat to the heat sink (T_h) and the second bed absorbs heat from the heat source (T_c). The heat rejection and heat absorption are achieved by two individual heat transfer loops, which are controlled by the corresponding valves and pumps. The cycle is completed by an internal heat recovery (HR) process driven by the temperature difference between the two beds, to precool the first bed from state 3 to state 4 and preheat the second one from state 6 back to state 1. HR is achieved by the third HTF loop controlled by the HR valve and pump (Qian et al., 2015a). In the previous test set up, NiTi tubes were used in each SMA bed, which were compressed on the axial direction of SMA tubes, as shown in Figure 1 (b). Water served as the HTF and flows inside those nitinol tubes for both heat transfer and heat recovery. The heat rejection loop was used to cool down each SMA bed to the heat sink's temperature T_h. The cooling delivery loop transfers generated cooling to the heat source, which was an electric heater in the test facility, denoted by T_c. During the heat recovery, water flows between two SMA beds without external heat transfer.

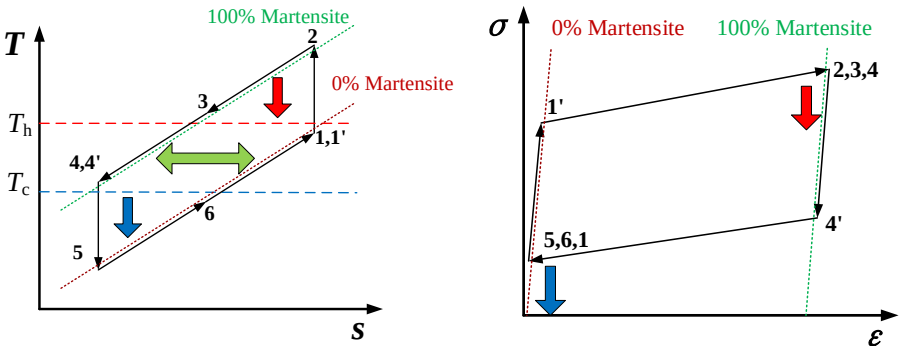

(a) Single-stage Brayton cycle

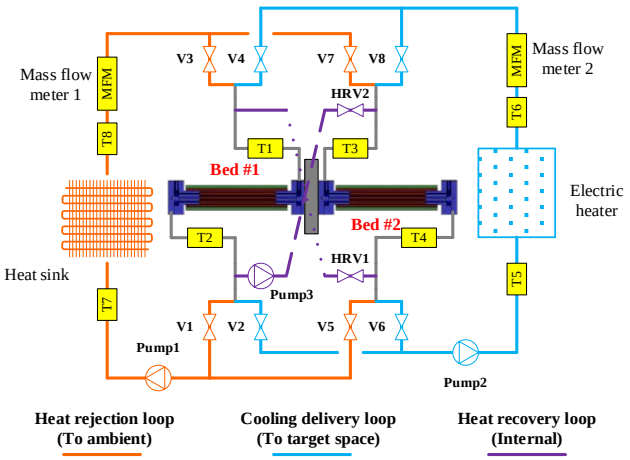

(b) Schematic of the single-stage prototype test facility

Figure 1: A single-stage elastocaloric cooling cycle in thermodynamic diagrams and schematic of the test facility.

2. PREVIOUS TESTS

In our previous work, we demonstrated preliminary test results using 7 ~ 10 NiTi tubes per SMA bed (Qian et al., 2015b). The phase transition required around 1,000 MPa stress, equivalent to 6.7 kN force for each tube. The tubes were compressed on their axial direction from both ends, by two loading heads as shown in Figure 2 (a). The two loading heads were used to compress the nitinol tubes, and distribute HTF through them as well. The bundle of nitinol tubes was surrounded by a tubes' holder, which prevented tubes from buckling while the tubes were compressed. The photo in Figure 2 (a) shows the entire nitinol tubes assembly working as a single SMA bed, which was supported and aligned by two linear bearings. Linear actuator was used to compress the two sets of SMA beds, which was driven by two servo motors. The frames, the linear actuator, the moving box and its supporting rails as well as the two nitinol tubes beds were assembled together, as shown in Figure 2 (b). As illustrated by Figure 1 (b), water was used inside all three HTF loops, controlled by ten solenoid valves and three pumps. T-type thermocouples were used to measure the in-stream water temperature, which were calibrated to have 0.2 K uncertainties. Two Coriolis mass flow meters were implemented to measure the flow rates of both the cooling HTF loop and heating HTF loop, with the calibrated accuracy of 0.2 g/s. Reported initial test results were 1.5 K system temperature lift and 38 W cooling capacity (Qian et al., 2015b).

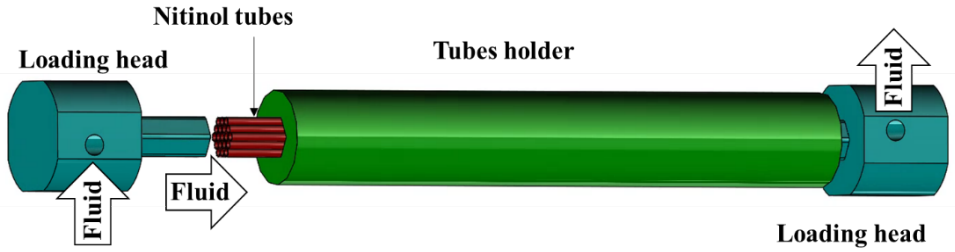

(a) Illustration of a single nitinol tube bed base assembly.

(b) Photo of the assembled prototype with motors

Figure 2: Illustration of the mechanically driven prototype. (Qian et al., 2015b).

3. NEW TEST RESULTS

3.1 Performance Enhancement Methods

Two novel designs were applied from literature (Qian et al., 2015c). As illustrated in Figure 3 (a), the first design was adding plastic insertions inside each Ni-Ti tube to reduce the dead thermal mass of the HTF and the associated cyclic loss. ABS plastic insertions made by the adhesive manufacturing technique (a.k.a. 3-D printing) were implemented in each Ni-Ti tube, which blocked approximately 50% of the flow cross sectional area, and reduced around 35% of the total dead thermal mass. The reduction in the cross section area corresponded to around a 20% pressure drop increase, which was a tradeoff for this design. The second novel design applied in the prototype was the plastic insulation tube design. Those PEEK (polyether-ether-ketone) plastic insulation tubes inside the loading head, between each Ni-Ti tube to the external HTF pipe, reduced the heat loss from the HTF to the metal loading head significantly. A graphic illustration of the plastic insulation tube concept is also shown in Figure 3 (b).

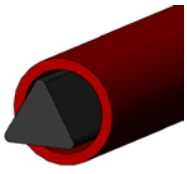

(a) Plastic insertion design

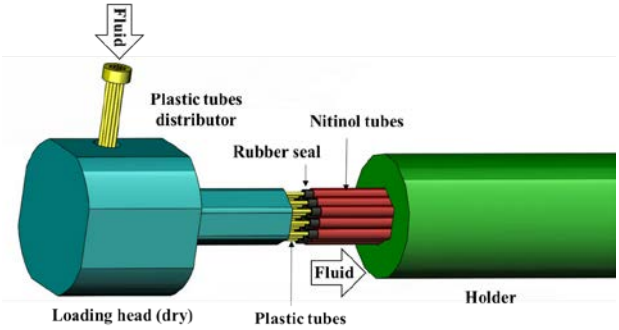

(b) Plastic insulation tube design

Figure 3: Illustrations of the plastic insertion and the plastic insulation tube designs.

3.2 Results and Discussions

With the two novel designs, we successfully achieved the maximum system temperature lift of 4.7 K. As illustrated by Figure 4, the system temperature lift was measured by the average water temperature difference between the heat sink side (TC7 and TC8) and heat source side (TC5 and TC6). The test was conducted under adiabatic condition, wherein both the heat sink (air-cooled fin-tube heat exchanger) and heat source (electric water heater) were well insulated, with no active cooling and electric heating. Since the input mechanical power gradually converted into heat via friction in the system, the overall temperature of fluid increased and eventually the system temperature lift saturated.

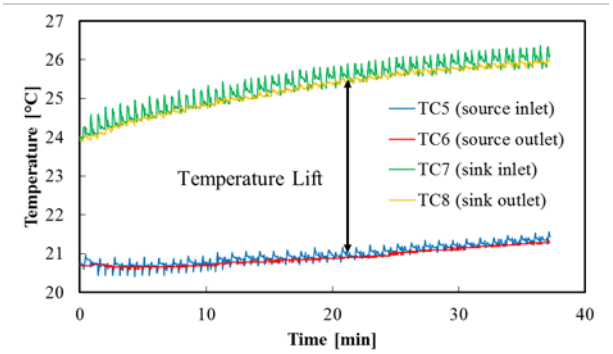

Figure 4: Demonstration of the fluid temperature variation over the testing period.

Figure 5 demonstrated the HTF temperatures measured at inlets and outlets of two SMA beds during one cycle. The obvious unsmooth temperature curves was a result of 2 Hz sampling frequency of data acquisition system. Though only the temperatures of the HTF were measured directly, the bed outlet temperatures echoed the variations of the SMA bed indirectly. Similar to the temperature variations in Figure 1 (a), the outlet temperature of bed 2 increased during the heat transfer process when HTF flowed inside the loaded NiTi tubes to reject heat at the beginning. The outlet temperature reduced under two different rates during heat transfer and heat recovery processes due to different heat transfer driving potential. Under the second half cycle, the NiTi tubes were unloaded. The water outlet temperature decreased first as a result of the unloaded latent heat. It increased during the HR process to preheat bed 2 before the next cycle began.

One observation from Figure 5 is the asymmetry of bed outlet temperatures between loading and unloading processes. For both beds, the temperature spike of the unloading bed occurred about two seconds earlier than the temperature spike of the loading bed. This is a result of the asymmetry in phase transformation speed because of work recovery. During the test, the work recovery was achieved by disengage the motor power to use one fully loaded bed to compress the fully unloaded bed. This process usually took less than 0.5 seconds. The remaining motor driven loading process took 1.5 seconds. Besides the asymmetry in phase change timing, more martensite turned back to austenite inside the unloading bed than the reverse phase transformation in the loading bed, due to hysteresis in the loading-unloading stress-strain relation. Consequently, most of the loading latent heat was released during the 1.5 seconds motor driven loading process and delayed the fluid temperature peak. In Figure 5, the fluid temperature variations during HR process indicated more than 50% HR efficiency, since fluid temperatures of bed 1 became above those of bed 2 at the end of the first HR process. In fact, based on the measured average fluid temperatures during the first HR process, the HR efficiency was 59%. The high HR efficiency was consistent with the measured HR efficiency from a previous study (Qian et al., 2015d). More efficient HR would reduce more cyclic loss from both the dead thermal mass of HTF remained inside the NiTi tubes and the thermal mass of the NiTi tubes, leading to more efficient system with better system temperature lift in the future.

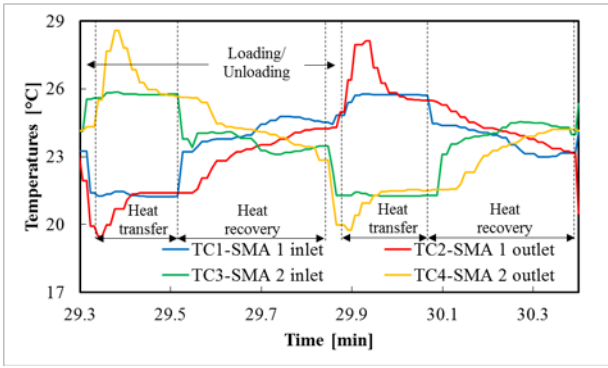

Figure 5: Inlets and outlets fluid temperature variations of two SMA beds during one cycle.

Based on the mass flow rate and fluid temperatures measured at the inlet and outlet of SMA bed 1, the instantaneous HTF heating and cooling capacities were obtained. Figure 6 (a) and Figure 6 (b) are plotted when the heat source and sink were turned off and on, respectively. As illustrated by Figure 6, the instantaneous heating capacity was above zero only during the heat rejection heat transfer process after the loading process. During the rest of the cycle, the heating capacity was zero because there was no HTF flowing between the heat rejection HTF loop and SMA bed 1. The instantaneous heating capacity gradually diminished to zero when approaching the end of the heat transfer process, due to less temperature difference between NiTi tubes and HTF towards the end of the heat transfer process. In addition, as can be found in Figure 5, the temperature peak after the loading process was delayed around two seconds after the unloading process, which resulted in negative heating capacity at the very beginning of the heat rejection period as shown in Figure 6. This negative instantaneous capacity neutralized part of the available heating capacity afterwards, and therefore, introduced more losses to the system. Such loss should always be minimized.

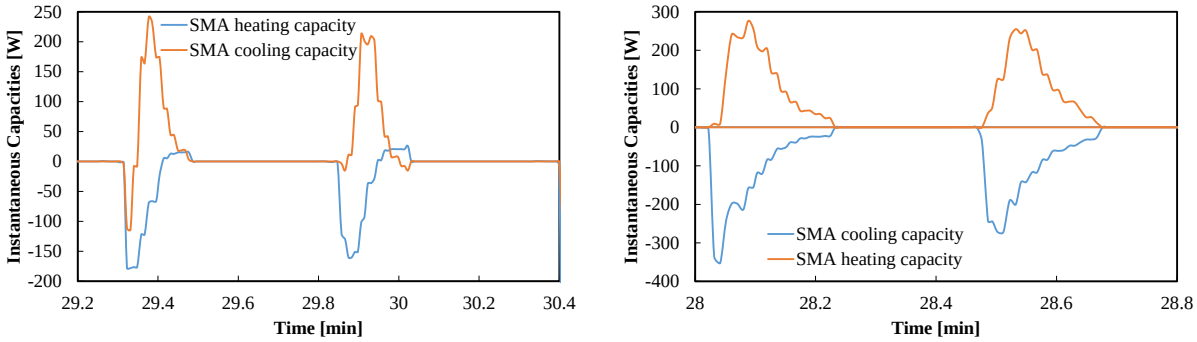

(a) Heat sink and heat source off, Q_c = 0 [W], ΔT_{lift} = 4.7 [K]

(b) Heat sink and heat source on, Q_c = 37 [W], ΔT_{lift} = 1.8 [K]

Figure 6: Instantaneous cooling/heating capacity of bed 1 measured by flow rate and fluid temperature difference.

However, the instantaneous heating and cooling capacities of the SMA heat sink and source were not identical to those of the SMA beds, as illustrated by Figure 7. The corresponding test conditions and time frame between Figure 6 and Figure 7 were consistent. The heat source side capacity already diminished to zero under the "adiabatic condition" when both the heat sink fan and heater were turned off, as shown in Figure 7 (a). Compared to the cooling capacity curve in Figure 6 (a), there was significant loss between the outlet of two SMA beds and inlet of the heat source. Based on the schematic in Figure 1, possible sources of loss can be summarized as follows:

(1) Heat generation from pumps. During the preliminary tests, a centrifugal pump was used, with an estimated heat generation rate of 12 W in the cooling HTF loop (Qian et al., 2015b). With the plastic insulation tube and plastic insertions, the HTF pressure drop increased, and a diaphragm pump consuming almost the same power replaced the old centrifugal pump. Therefore, the pump neutralized around 12 W cooling capacity.

(2) Cyclic loss caused by unavoidable fluid mixing. The junction between heating HTF, cooling HTF and HR loop may generate this fluid mixing. In the prototype, all the water loops were constructed in close loops, without

expansion tank or constant pressure point, leading to drastic pressure variations inside the system. Most of the hoses were steel reinforced, however, might still suffer slight volumetric variations, which eventually resulted in unnecessary heating/cooling/HR fluid mixing. Reducing the length of the HTF pipes, using more rigid pipe materials may reduce this loss.

(3) Convective heat loss to the ambient. Since the HTFs' temperatures was below room temperature, there was continuous heat transfer from ambient to heat up the HTF. During the tests, all the HTF tubes and hoses were well insulated by more than 1 cm thick polymer pipe insulation layer. Therefore, the major heat loss to the ambient was from the accessories, such as valves and mass flow meters.

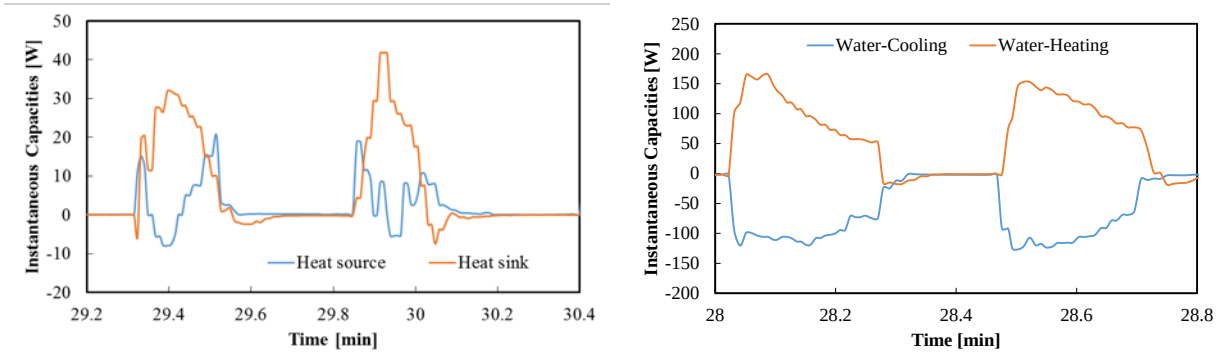

(a) Heat sink and heat source off, Q_c = 0 [W], ΔT_{lift} = 4.7 [K]

(b) Heat sink and heat source on, Q_c = 37 [W], ΔT_{lift} = 1.8 [K]

Figure 7: Instantaneous cooling and heating capacities of heat sink and heat source.

To quantitatively identify the contribution of each loss, Table 1 compared the time averaged cooling capacity of heat source (Q_c), the SMA instantaneous capacity (in Figure 6), and the time average SMA capacity. Whether the heater was on or off, there is a consistent 10 ~ 20 W capacity difference between Q_c and SMA bed's capacity, which is the overall loss. Since the pump's heat generation was estimated to be 12 W, loss (2) and loss (3) together accounted for the rest 0 ~ 8 W heat loss. The SMA bed's time average capacity can be converted to the mass based cooling density transferred from the SMA, which ranged from 5.6 J/g to 10.2 J/g. Compared with the latent heat of NiTi, i.e. 12 J/g, more latent heat could be transferred to HTF under small temperature lift conditions as a result of less cyclic loss. Though HR reduced the cyclic loss, its efficiency was always less than 100%. Consequently, only 47% latent heat was transferred to HTF under the maximum temperature lift condition.

Table 1: Comparison of the instantaneous cooling capacity measured by SMA bed and heat source.

Heater /sink	ΔT_{ad} [K]	Heat source Q_c [W]	SMA max instantaneous cooling capacity [W]	SMA time average cooling capacity [W]	SMA mass based cooling density [J/g]
Off	4.7	0	177	19	5.6
On_1	1.8	37	352	55	8.9
On_2	0.1	65	293	78	10.2

We have varied the cycle duration from 10 seconds to 30 seconds, varied the HR flow rate, and heater and sink's loads to measure the system performance under a wide range of conditions. Figure 8 summarized the highlighted test results. The diamond points are baseline test results (Qian et al., 2015b), wherein no enhancement methods were applied. With the PEEK plastic tubing insulation design from Figure 3 (b), heat loss inside the SMA bed from HTF to the metal loading heads was reduced, achieved 2.8 K system temperature lift and 41 W cooling capacity. By upgrading the motor assembly with a gearbox, three more NiTi tubes were inserted into each SMA bed, increasing the system cooling capacity. It should be noted that though the system cooling capacity was increased from 41 W to 65 W, the mass based capacity of 0.5 ~ 0.6 W/g-NiTi was barely changed. Theoretically, the maximum temperature lift of 2.8 K should remain the same when changing 7 tubes per bed to 10 tubes per bed. The only reason leading to the change of temperature lift from 2.8 K to 4.2 K was due to the reduction of the ratio between dead thermal mass (loss) and the active NiTi's thermal mass, i.e. the dead thermal mass of HTF remained almost constant in each SMA bed within the three loops' junction while the active thermal mass of NiTi increased by almost 43%. This also indicated that the dead thermal mass of HTF, its pipe and metal supporting parts such as loading heads and holder should be further reduced. Furthermore, by adding plastic insertions inside each NiTi tube, the system temperature

lift was increased to 4.7 K. In addition, a projection was made assuming the aforementioned 20 W heat loss in Table 1 could be totally saved, which resulted in the maximum projected cooling capacity of 85 W, and maximum projected system temperature lift of 6.1 K. Nevertheless, the 20 W heat loss itself was more than 30% of the maximum cooling capacity achieved in the prototype, which definitely to be overcome through more studies.

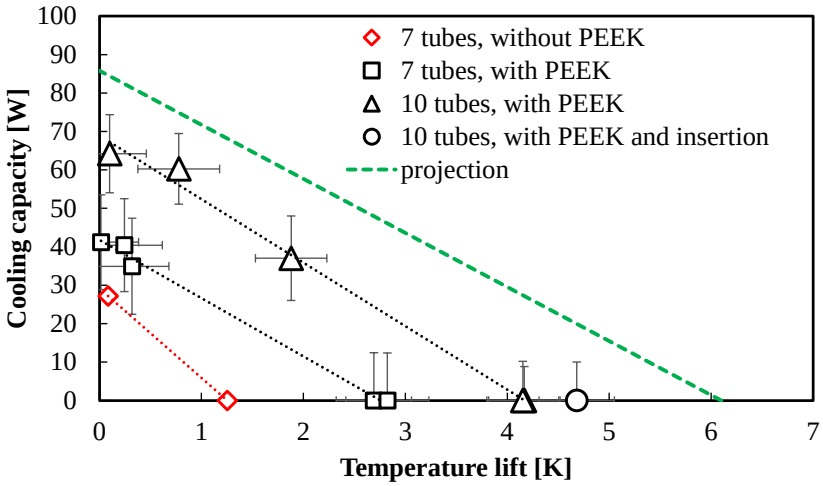

Figure 8: Highlighted test results.

4. CONCLUSIONS

In this study, we demonstrated the latest test results achieved from the world's first of-its-kind compressive elastocaloric cooling prototype. Two novel designs were implemented into the system, and the motor assembly was upgraded to enable more NiTi tubes per SMA bed. Consequently, the system temperature lift was successfully improved up to 4.7 K, and 65 W cooling capacity. It was found that there was a consistent cooling capacity difference of 10 ~ 20 W between the output cooling power from SMA bed and achieved cooling power measured from the heat source, wherein the pump heat generation contributed to most of it. Other factors should be minimized as well, including the heat loss to ambient and unnecessary fluid mixing when switching the valves. Future studies and prototypes should keep addressing these losses, especially the cyclic losses caused by the dead thermal masses of HTF and supporting parts, which are still major obstacles limiting the system temperature lift and cooling capacity.

NOMENCLATURE

COP	coefficient of performance	(–)
HR	heat recovery	
HTF	heat transfer fluid	
PEEK	polyether-ether-ketone	
Q_c	cooling capacity	(W)
SMA	shape memory alloys	
s	specific entropy	($J \cdot g^{-1} \cdot K^{-1}$)
T_c	heat source temperature	(°C)
T_h	heat sink temperature	(°C)
ΔT_{lift}	system temperature lift	(K)
σ	stress	(MPa)
ε	strain	(–)

REFERENCES

Goetzler, W., Zogg, R., Young, J., Johnson, C., 2014. Energy savings potential and RD&D opportunities for non-vapor compression HVAC technologies.

Ossmer, H., Miyazaki, S., Kohl, M., 2015. Elastocaloric heat pumping using a shape memory alloy foil device. 2015 *Transducers*, Anchorage, USA.

Qian, S., Ling, J., Hwang, Y., Radermacher, R., Takeuchi, I., 2015a. Thermodynamic cycle analysis and numerical modeling of thermoelastic cooling systems. *Int. J. Refrigeration*, 56, 65-80.

Qian, S., Wu, Y., Ling, J., Muehlbauer, J., Hwang, Y., Takeuchi, I., Radermacher, R., 2015d. Design, development and testing of a compressive thermoelastic cooling prototype. *International Congress of Refrigeration* 2015, Japan. Paper 0092.

Qian, S., Alabdulkarem, A., Ling, J., Muehlbauer, J., Hwang, Y., Radermacher, R., Takeuchi, I., 2015c. Performance enhancement of a compressive thermoelastic cooling system using multi-objective optimization and novel designs. *Int. J. Refrigeration*, 57, 62-76.

Qian, S., Ling, J., Muehlbauer, J., Hwang, Y., Radermacher, R., 2015d. Study on high efficient heat recovery cycle for solid-state cooling. *Int. J. Refrigeration*, 55, 102-119.

Qian, S., Geng, Y., Wang, Y., Ling, J., Hwang, Y., Radermacher, R., et al, 2016. A review of elastocaloric cooling: materials, cycles and system integrations. *Int. J. Refrigeration*, 64, 1-19.

Saylor, A., 2012. ARPA-E summit technology showcase. http://www.energy.gov/articles/2012-arpa-e-summit-technology-showcase (Retrieved on Nov. 12, 2015)

Schmidt, M., Schutze, A., Seelecke, S., 2015. Scientific test setup for investigation of shape memory alloy based elastocaloric cooling processes. *Int. J. Refrigeration*, 54, 88-97.

Tusek, J., Engelbrecht, K., Solsona, R.M., Manosa, L., Vives, E., Mikkelsen, L.P. et al., 2015. The elastocaloric effect: a way to cool efficiently. *Adv. Energy Mater*, 1500361.

ACKNOWLEDGEMENT

The authors gratefully acknowledge the support of this effort from the U.S. DOE (ARPA-E DEAR0000131) and the Center for Environmental Energy Engineering (CEEE) at the University of Maryland. The authors would also appreciate the heat sink donated by Thermatron Inc.